Two-Dimensional Crystallization on Lipid Monolayers and Three-Dimensional Structure of Sticholysin II, a Cytolysin from the Sea Anemone *Stichodactyla helianthus*

Jaime Martín-Benito,* Francisco Gavilanes,† Vivian de los Ríos,† José M. Mancheño,† José J. Fernández,‡ and José G. Gavilanes†

*Centro de Microscopía Electrónica "Luis Brú," Universidad Complutense, 28040 Madrid; †Departamento de Bioquímica y Biología Molecular I, Universidad Complutense, 28040 Madrid; and ‡Departamento de Arquitectura de Computadores y Electrónica, Universidad de Almería, 04120 Almería, Spain

ABSTRACT Sticholysin II (Stn II), a potent cytolytic protein isolated from the sea anemone *Stichodactyla helianthus*, has been crystallized on lipid monolayers. With Fourier-based methods, a three-dimensional (3D) model of Stn II, up to a resolution of 15 Å, has been determined. The two-sided plane group is $p22_12$, with dimensions $a = 98$ Å, $b = 196$ Å. The 3D model of Stn II displays a Y-shaped structure, slightly flattened, with a small curvature along its longest dimension (51 Å). This protein, with a molecular mass of 19.2 kDa, is one of the smallest structures reconstructed with this methodology. Two-dimensional (2D) crystals of Stn II on phosphatidylcholine monolayers present a unit cell with two tetrameric motifs, with the monomers in two different orientations: one with its longest dimension lying on the crystal plane and the other with this same axis leaning at an angle of ~60° with the crystal plane.

INTRODUCTION

Sea anemones produce a number of toxic peptides and proteins within intracellular specialized organelles called nematocysts for defensive and predatory purposes. Among these toxins, more than 20 potent cytolytic proteins have been isolated and characterized (Harvey, 1990). These cytolysins exhibit many common features: they consist of a single polypeptide chain with a molecular mass of 15–20 kDa, with basic character (pI ranging from 8 to12), a high chemical stability, and a high affinity toward sphingomyelin (see reviews in Bernheimer, 1990; Harvey, 1990; Turk, 1991; Macek, 1992). In addition, a high degree of amino acid sequence similarity has been found among these cytolysins (Blumenthal and Kem, 1983; Simpson et al., 1990; Belmonte et al., 1994). These toxins produce massive cytolytic effects on erythrocytes, platelets, and fibroblasts (Kem, 1988; Bernheimer, 1990; Norton, 1991; Turk, 1991), and it has been suggested that the lysis occurs by formation of oligomeric pores, which would cause a colloid osmotic shock. This hypothesis is based on the results from different studies performed with lipid model membranes (Michaels, 1979; Varanda and Finkelstein, 1980; Zorec et al., 1990; Belmonte et al., 1993; Tejuca et al., 1996; de los Ríos et al., 1998).

One of the most studied sea anemones is *Stichodactyla helianthus,* occurring in the coastal waters of the Caribbean regions. The toxic components of the venom of this anemone can be divided into low-molecular-mass (3–5 kDa) neurotoxins acting on sodium channels (Castañeda et al., 1995) and cytolysins belonging to the above-mentioned group (Bernheimer and Avigad, 1976; Tejuca et al., 1996; de los Ríos et al., 1998). Sticholysin II (Stn II) is one of these cytolytic proteins. It has a molecular mass of 19.2 kDa with 175 amino acid residues, and it is closely related to other toxins such as equinatoxin II, from *Actinia equina* (Belmonte et al., 1994), and tenebrosin C, from *Actinia tenebrosa* (Simpson et al., 1990). Studies of leakage of encapsulated solutes induced by Stn II on model membranes have shown that the maximum extent of leakage is dependent on the molecular mass of the vesicle-entrapped solute, suggesting the involvement of transmembrane pores in the permeabilization process (de los Ríos et al., 1998). Moreover, kinetic analysis of the leakage process points to the existence of protein-protein interactions as a requirement for the leakage to be triggered. A similar picture has been proposed for equinatoxin II, which would form cation-selective channels composed of several monomers (Zorec et al., 1990; Belmonte et al., 1993; Macek et al., 1995). In this regard, we have recently shown that Stn II behaves in solution as an associating monomer-tetramer system (de los Ríos et al., 1999), revealing the propensity of Stn II to aggregate, forming discrete oligomeric species. In this work, we show that Stn II forms two-dimensional (2D) crystals on lipid films by using the method developed by Fromherz (1971) and Uzgiris and Kornberg (1983). This methodology has made it possible to visualize tetrameric species in a membrane-like environment, and a model of the 3D structure of Stn II has been derived by analyzing the images of tilted negatively stained crystals.

MATERIALS AND METHODS

Stn II has been isolated as previously described (de los Ríos et al., 1998) from extracts of specimens of *S. helianthus* (purchased from Nayeco,

Received for publication 20 September 1999 and in final form 28 February 2000.

Address reprint requests to Dr. Jaime Martín-Benito, Centro Nacional de Biotecnología, Consejo Superior de Investigaciones Científicas, Universidad Autónoma de Madrid, 28049 Madrid, Spain. E-mail: jmartinb@cnb.uam.es.

0006-3495/00/06/3186/09 $2.00

Barcelona, Spain), prepared by mincing and homogenizing the whole sea anemone body. Briefly, the purification procedure includes gel filtration chromatography on a Sephadex G-50 column equilibrated in 20 mM ammonium acetate (pH 5.0). The fractions with the highest hemolytic activity were pooled, dialyzed, and loaded onto a CM-cellulose CM-52 column equilibrated in 0.1 M ammonium acetate (pH 5.0). The protein was eluted by using a 0.1–0.4 M ammonium acetate linear gradient. This ion-exchange chromatography renders two well-resolved hemolytic peaks, Stn II being the more basic one. This procedure renders sequence grade purified protein (de los Ríos et al., 1998).

Stn II crystals on lipid monolayers were obtained in a Teflon well (3.5-mm diameter and 2.0-mm depth) by incubating 12 μl of 1 mg/ml protein sample in Tris buffer (10 mM Tris, pH 7.0, containing 0.1 M NaCl and 1 mM EDTA), and 2–3 μl of a solution of the corresponding lipid dissolved in chloroform:methanol (2:1, v/v), at 1 mg/ml total lipid concentration. The composition of monolayers herein considered was the following: bovine brain sphingomyelin, egg phosphatidylcholine, and a mixture of egg phosphatidylcholine:cholesterol (3:1, w/w). All of these lipids were purchased from Avanti Polar Lipids (Alabaster, AL). Incubation was carried out either at room temperature or at 4°C in a sealed humid chamber, and the time was varied from 2 to 7 h. Under these conditions, the protein spontaneously interacts with the lipid monolayer. The crystals were sampled by using 200-mesh hexagonal copper electron microscope grids coated with colodion holey film and with recently evaporated carbon (Kubalek et al., 1991). The grid was gently placed on the surface of each well for 2 min. When it was withdrawn, the excess liquid was blotted with filter paper. Afterward, the samples were negatively stained for 1 min with 2% (w/v) uranyl acetate or 0.5% glucose:0.5% uranyl acetate. The grids were blotted again and left to completely dry before observation. Controls in the absence of lipids were also performed. In these cases, flat structures lacking crystalline order were observed (not shown). Because sea anemone cytolysins have been demonstrated to be surface active (Doyle et al., 1989), these structures could correspond to protein monolayers formed at the air-water interphase.

The grids were examined on a Zeiss EM-902 (80-kV) transmission electron microscope (Carl Zeiss; Oberkochen, Germany). Micrographs were taken under low-dose conditions by using the minimum dose focusing system at a calibrated magnification of 49,000× and a nominal underfocus of 2000–4000 Å. A total of six tilt series of crystals, five stained with uranyl acetate and one with glucose:uranyl acetate, were recorded from −45° to +45° at intervals of 5°. In all cases, two projections at 0°, taken at the beginning and at the end of the series, were used to evaluate the radiation damage in the crystals.

The image quality and the crystalline order were evaluated by using CRISP software (Hovmöller, 1992), version 1.7f. The best micrographs were digitized with an Eikonix-1412 Digital Camera (Kodak, Rochester, NY) at a resolution of 4.5 Å/pixel and processed with the MRC Image Processing Programs (Crowther et al., 1996) implemented in a Silicon Graphics workstation (Mountain View, CA). This process includes the correction of distortions by correlation and averaging methods (Henderson et al., 1986). Briefly, the procedure involves a quasioptical filtering of the Fourier-transformed original image. A part of this filtered image was boxed off to provide a reference area, which was used to calculate a cross-correlation map against the whole image area. The cross-correlation map allows the calculation of a distortion map that permits correction of the crystal deformations. After the unbending process, the crystal was weighted in function of crystallinity (Baldwin et al., 1988), thus eliminating the poorly ordered areas and incrementing the signal-to-noise ratio in the Fourier transform of the corrected image. Finally, the contrast-transfer function was determined by ICE software (Hardt et al., 1996). The image size was 2000 × 2000 pixels and contained ~200–400 unit cells after the correction of distortions (Henderson et al., 1986) and weighting in function of crystallinity (Baldwin et al., 1988). The final three-dimensional (3D) images were generated with CRISP-Triview software.

RESULTS

Influence of the monolayer composition on crystal growth

The composition of the lipid monolayer was the most important factor in determining crystal quality. The crystallization was carried out with monolayers with three different compositions: bovine brain sphingomyelin (SM), egg phosphatidylcholine (PC), and a 3:1 mixture (w/w) of egg phosphatidylcholine:cholesterol (PC:chol). Attempts to obtain crystalline structures with monolayers composed of SM were unsuccessful; complex amorphous structures like "tangles" were found in most observations. In very few cases (less than 5%), small crystalline arrays appeared, showing a Fourier transform with one or two diffraction orders in a hexagonal pattern of a close-packed structure. These results were practically independent of the incubation conditions. For monolayers composed of 3:1 PC:chol, crystalline patches were observed in 5–10% of the total areas. The computer processing of the images obtained from these patches showed a structure where only three or four diffraction orders (up to 25–30 Å) were at most clearly visible. In this case, the crystallization conditions influenced only the number of crystals but scarcely affected their quality. Finally, the monolayers composed of PC induced crystals of good quality; Fig. 1 shows an example of such crystals. The abundance of crystalline patches was up to 20%, and the power spectrum was clearly revealed until the eighth or ninth diffraction order (up to 15 Å), making these crystals suitable for three-dimensional (3D) reconstruction. Optimization of the crystallization conditions resulted in an increase in the number, size, and quality of the crystals for up to 5 h of incubation; longer periods did not induce the formation of better crystals.

A common feature in all of our observations was that the crystals were usually found across the holes and seldom on the carbon matrix. Nevertheless, the crystals remained stable without moving or rearranging under the beam irradiation, despite their presence in the holes. When we used conventional carbon-coated grids (not holey), the results were unsatisfactory: the samples appeared "dirty," without crystalline areas. Similar behavior has previously been reported (Kubalek et al., 1991; Taylor and Taylor, 1993; Voges et al., 1994).

Projection structures and plane group determination

Fig. 1 shows a typical 2D crystal of Stn II obtained on a PC monolayer, as well as its computed diffraction pattern. From the Fourier transform, it is clear that the spacing in the crystal lattice is exactly two times larger in one direction than in the other. The projection map obtained without any symmetry imposition appears in Fig. 2 *a*. This map reveals

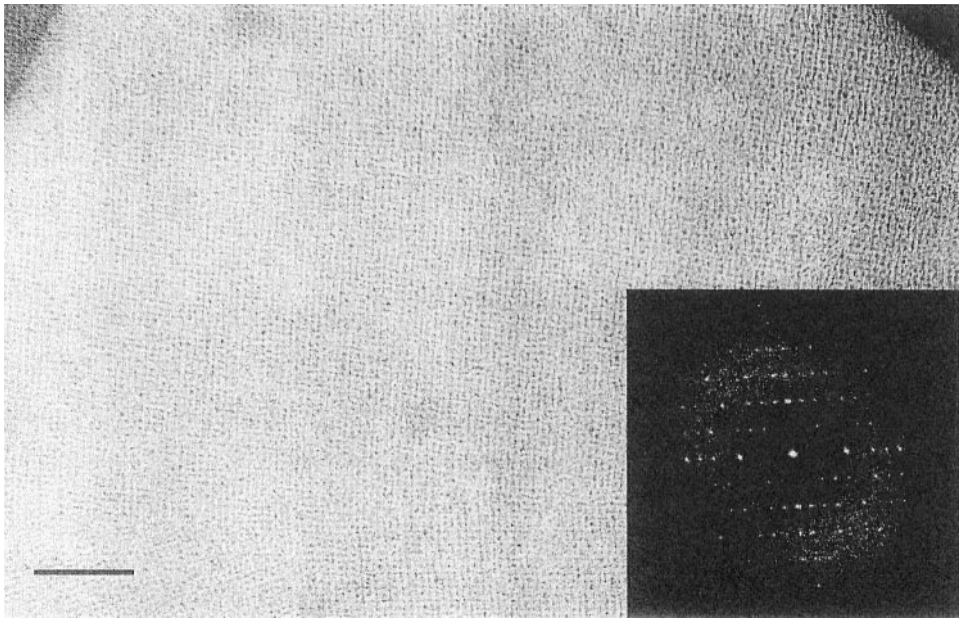

FIGURE 1 Two-dimensional crystal of Stn II on monolayers composed of egg PC. The crystal was negatively stained with uranyl acetate 2% (w:v). The support was a carbon-coated holey film. The inset shows the computed diffraction pattern after the complete processing of the image; a spacing ratio of 2:1 between the crystallographic axes can be observed. The scale bar represents 100 nm.

two tetrameric motifs; of the molecules forming the motifs, the opposing two have a similar appearance. The two tetrameric structures have the same size but their aspect is slightly different, being arranged in alternating columns.

To determine the space group, the programs ALLSPACE (Valpuesta et al., 1994) and CRISP (Hovmöller, 1992) were used. Table 1 shows phase residuals of the allowed space groups for the crystal ($\gamma = 90°$) obtained using ALLSPACE; the smaller values correspond to p2, p12, and $p22_12$ groups. Because the residual differences are very low, the $p22_12$ group should be chosen because of its highest symmetry (Valpuesta et al., 1994). In fact, p2 and p12 are maximal nonisomorphic subgroups of $p22_12$, and the combination of the symmetry operators present in these groups originates the $p22_12$ group; that is, p2 and p12 have fewer phase restrictions, and their phase residuals always will be smaller than those of the $p22_12$ group. In addition, $p22_12$ was the symmetry selected by CRISP software.

Fig. 2 *b* shows the $p22_12$ symmetrized projection structure. The imposition of $p22_12$ symmetry (and p12) implies the equalization of the projection of the two tetrameric structures. However, the analysis of more than 100 micrographs of many different crystals, grown under varying conditions and stained with either uranyl acetate or a mixture of glucose and uranyl acetate, always produced projection maps very similar to the one shown in Fig. 2 *a*, with two slightly different motifs. The origin of this difference was attributed to an incomplete staining of a single type of asymmetrical tetramer, but placed in inverted positions. This incomplete staining is probably due to the interaction of the protein with the monolayer (see Discussion). The symmetry of the $p22_12$ two-sided plane group implies the presence of twofold screw axes along the longest lattice vector (Fig. 2 *b*), which arranges the tetramers facing upward and downward in alternate columns. In this way, and because of a potential incomplete staining, the projections should show the upper and lower parts of the same structure.

Three-dimensional reconstruction

Because of the higher quality of the crystals obtained on PC monolayers, these samples were chosen to take tilt series. After the selection of the best series, the tilt parameters were calculated by using the Shaw and Hills formulas (1981).

The resolution of each micrograph was estimated by using the method developed by Henderson et al. (1986). Basically, this method divides the Fourier transform into concentric crowns and calculates the mean value for all of the spots inside. If this mean value is higher than the mean noise background, it is assumed that the resolution of this crown has been reached. After correction of the lattice distortions, the untilted image showed a resolution of 15 Å. The remaining tilted micrographs used in the 3D reconstruction were in the range of 15–18 Å (14 micrographs) and 20 Å (two micrographs). The evaluation of the radiation damage was carried out by comparing the resolution of the first image—without tilt—and the last image, obtained after the complete tilting set, also at 0° tilt. The two images reached the same resolution (15 Å), although the last micrograph showed a slight attenuation of the higher frequencies as a consequence of slight radiation damage. Hence, no significant beam damage, which would influence the model at the expected resolution, was produced.

To calculate the crystal thickness, a first approximation was made based on the projection area and the molecular

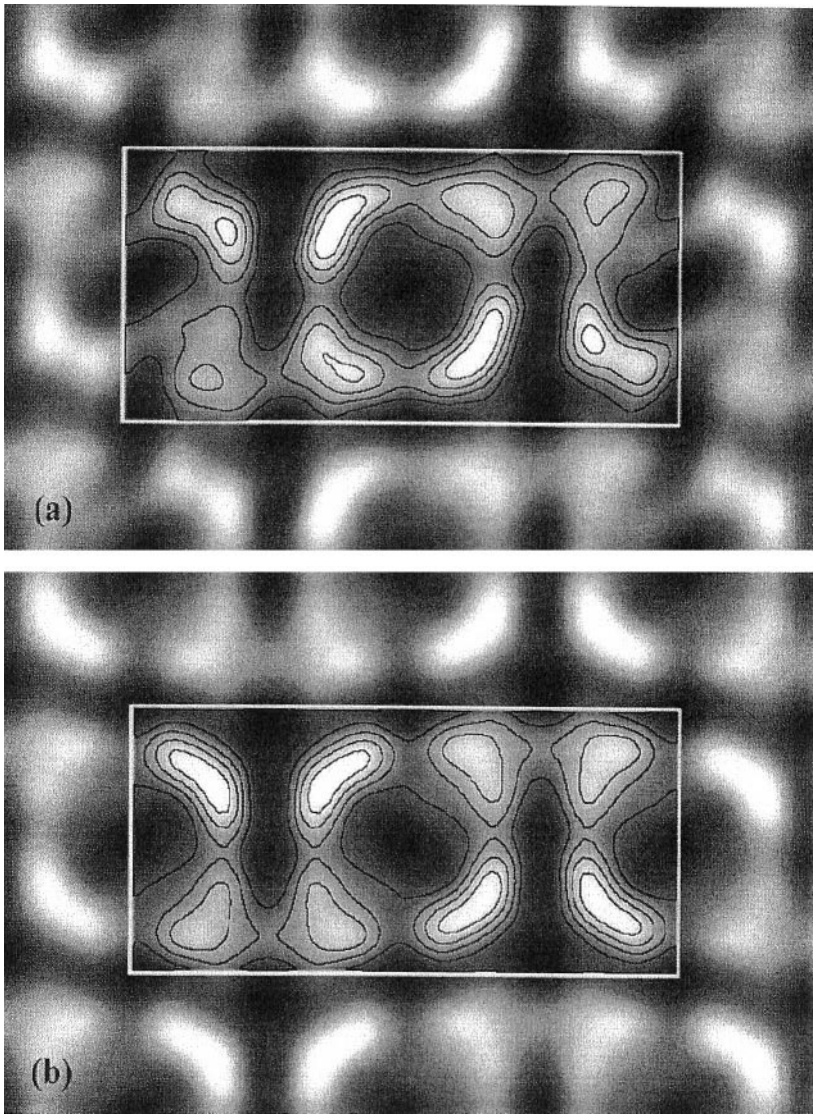

FIGURE 2 Fourier maps of crystals of Stn II. (*a*) Projection map obtained from Fig. 1 without the imposition of any symmetry. The unit cell dimensions are 98 Å × 196 Å, gamma = 89.1°; it contains eight molecules of protein arranged in two tetrameric structures of the same size. (*b*) Projection map after application of the $p22_12$ symmetry.

mass of the protein, assuming a mean protein density of 0.85 Da/Å^3. From this approach, we have found that the thickness should be in the 30–70-Å range, depending on the projection chosen to perform the calculations. In this work, we were able to make a more precise estimation of the thickness because the final 3D reconstruction showed the protein in two orientations (see below).

The common phase origin refinement was performed with the program ORIGTILT (Amos et al., 1982). Fig. 3 shows some projection maps with the tilt angle indicated. The lattice lines obtained after phase origin alignment and amplitude scaling showed a good fitting, and some special characteristics of the $p22_12$ space group are remarkable in these lines (Fig. 4). The mean value of phase residual obtained from origin refinement was 31.6° up to 15 Å.

The 3D structure of the unit cell consists of two tetrameric motifs placed facing upward and downward, respectively (Fig. 5), both related by screw axes parallel to the crystal plane. Following the distribution of the lobes marked in this figure, it is clear that the proteins are placed in two orientations. One shows the molecule with its longest axis (51 Å) lying on the crystal plane and the concave face toward the center of the tetramer. The other position places the protein with this longest axis leaning at an angle of ~60° with the crystal plane and the concave face toward the outer part of the oligomer.

The fact that the proteins are placed in two orientations has two advantages in this context: 1) it is possible to make an accurate estimation of the crystal thickness from the projection map without tilting; 2) the two orientations show two views of the same protein, providing an excellent internal control that permits us to verify that the selection of the $p22_12$ group is correct. These two volumes constitute the asymmetric unit cell; that is to say, they are not related by any symmetry operator, although they are very similar, which points out the density map quality.

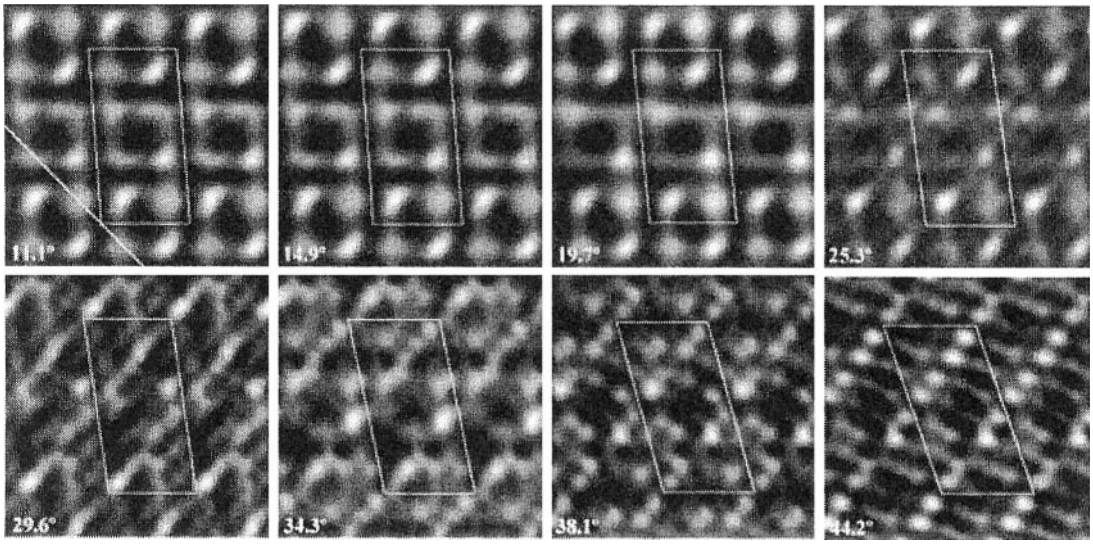

FIGURE 3 Projection maps of the tilt series after phase origin alignment. The actual tilt angles are indicated. The unit cell is drawn for each image, and the tilt axis is marked in the first map.

The structure of the protein monomer appears in Fig. 6. The 3D molecular envelope of Stn II shows a protein that is slightly flattened, warping, and three-lobed; one of these lobes is smaller than the others. The longest dimension is 51 Å (the distance between the extremes of the biggest lobes), and the maximum width of the main body is ~40 Å (including the smallest lobe).

DISCUSSION

2D Crystallization

Stn II belongs to a family of toxins that spontaneously interact with natural and model membranes. This interaction probably occurs through a nonspecific binding of the protein to the lipids (de los Ríos et al., 1998). In this study we have found that Stn II interacts with monolayers of different compositions, supporting the nonspecific nature of the interaction. Our results have also shown the ability of the protein to form well-ordered 2D crystals on lipid monolayers, which are suitable for 3D reconstruction. The possibility of 3D crystal formation was discarded because no extinction due to Bragg law was observed and continuous lattice lines were obtained after the complete analysis of tilted images.

TABLE 1 Internal phase residuals of all possible plane groups ($\gamma = 90°$, $a \neq b$, and primitive cell) from the best image

Plane group	Phase residual versus other spots (90° random)	No. of comparisons	Phase residual versus theoretical (45° random)	No. of spots
p1	18.7*	150	13.5	150
p2	26.6†	75	13.3	150
p12_b	35.1	54	33.4	16
p12_a	77.0	50	51.2	8
$p12_1$_b	23.7‡	50	8.7	8
$p12_1$_a	69.0	54	45.2	16
p222	59.1	179	13.4	150
$p22_12$	28.5‡	179	13.3	150
$p222_1$	60.9	179	13.3	150
$p22_12_1$	61.8	179	37.1	150

*Theoretical phase residual based on the signal-to-noise ratio of the observed diffraction spots.
†Acceptable.
‡Should be considered.

The image analysis of these 2D crystals shows a relationship between the quality of the crystals and the composition of the monolayer. For monolayers composed of SM, close-packed or noncrystalline complex structures have been obtained. When PC:chol mixtures were used, the crystals were poorly ordered; but, for PC monolayers, the quality of the crystals was good. Because the affinity of protein for these lipids is SM $\gg$ PC:chol $>$ PC (Macek, 1992), it seems clear that there is an inverse relationship between the quality of crystals and the affinity for the lipid of the monolayer. The chemical differences between PC and SM are limited to the nonpolar region, PC has two fatty acid chains esterifying glycerol, while SM has a ceramide moiety; the polar group is choline in both cases. In this way, the part of the monolayer exposed to the protein-containing aqueous solution is the same for PC and SM. These data suggest that the differences in the crystalline array quality may not be due to the initial steps of the protein-lipid interaction, but to the ability of Stn II to rearrange in 2D crystals after such initial steps. For pure SM monolayers, this capability seems to be very low, almost nil. Accordingly, de los Ríos et al. (1998) have shown that the leakage induced by Stn II on PC:SM vesicles increases with the percentage of SM, reaching a

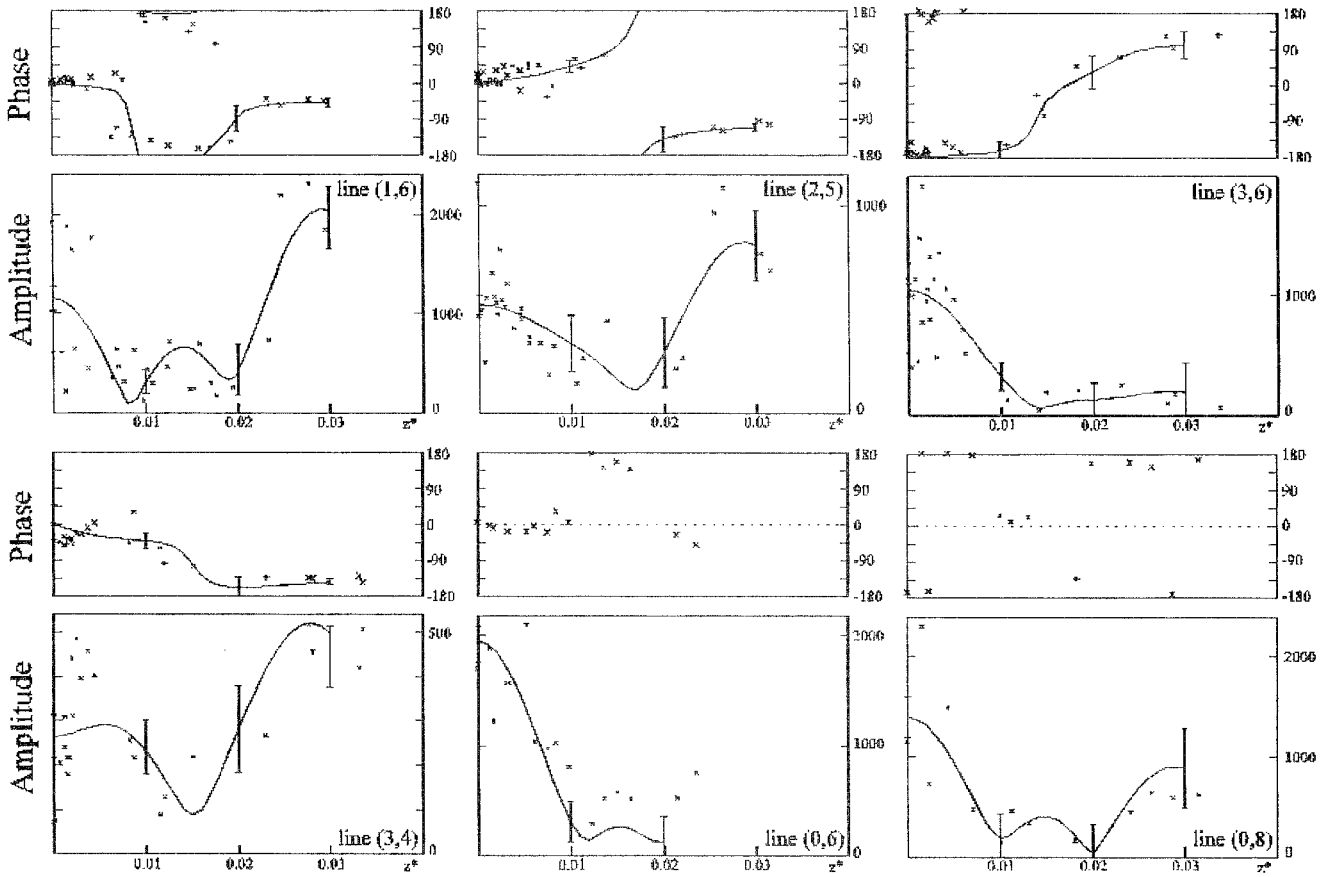

FIGURE 4 Variation of phases (*top*) and amplitudes (*bottom*) along some reciprocal lattice lines. The reflections presented are (1, 6), (2, 5), (3, 6), (3, 4), (0, 6), and (0, 8). Most of the experimental data of the lines (0, 6) and (0, 8) clearly show the special characteristics of the $p22_12$ group symmetry, where the phases of the lines (0, k, l) (k = even) are constrained to values of 0° or 180°.

maximum at a PC:SM ratio of ~4:1. These results raise the possibility that the high affinity of Stn II for SM could be an essential factor that somehow modulates the steps leading to the final competent structure that permeabilizes membranes. Consequently, an excess of SM produces a very strong lipid-protein interaction that prevents the protein rearrangements leading to pore formation. This hypothesis could explain the fact that SM-pretreated Stn II is inactive in the assays against erythrocytes or model membranes (Bernheimer and Avigad, 1976). The comparison of the results obtained with PC and PC:chol monolayers could also be interpreted in similar terms. The presence of cholesterol would affect the nonpolar region of the monolayer, changing its fluidity by modulating the molecular motion of the phospholipid acyl chains, and it could modify the protein rearrangement ability after the initial interaction.

Plane group determination

The analysis of the crystals shows that the two-sided plane group is $p22_12$. The slight difference between the projections of the two tetrameric structures in all of the micrographs is most probably a consequence of an incomplete staining. This incomplete staining could arise for the following reasons: 1) the large size of the protein prevents the complete staining; 2) the tetramers are placed at different levels; and 3) the proteins that compose the tetramers are partially protected by the monolayer. The first possibility should be discarded because the protein has 175 amino acids, its maximum length is 51 Å, and its width is 40 Å, according to the final 3D reconstruction. Moreover, the difference between the two projections remains when we use glucose:uranyl acetate, a mixture that allows for the contrast of a greater height of specimen because of the sugar viscosity. The second possibility should also be rejected because the final 3D reconstruction presents two motifs at the same level, and this is an actual feature of the structure and not a consequence of the symmetry application. In addition, the crystallization on lipid monolayers involves the interaction of proteins with a plane surface and the chances of obtaining structures at different levels are reduced. Therefore, partial protection of the protein by the monolayer is the most plausible explanation for the incomplete staining. This hypothesis is based on the fact that Stn

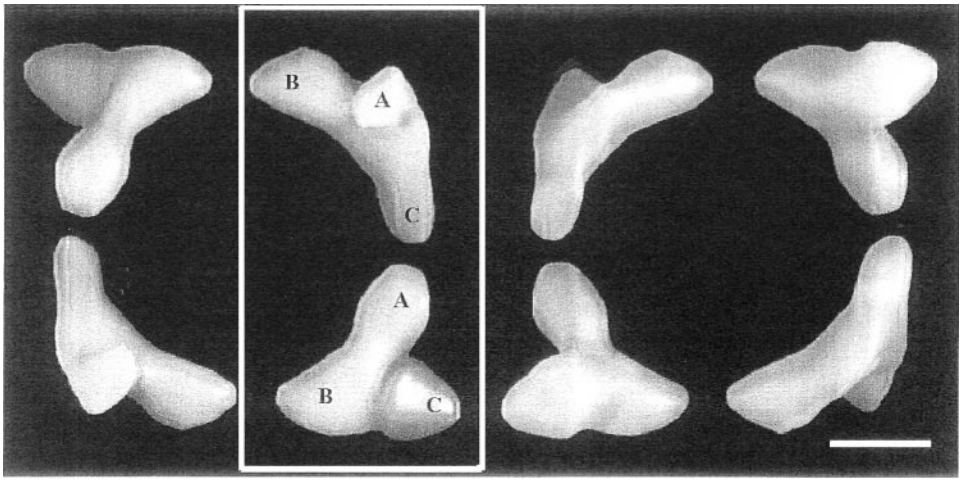

FIGURE 5 Three-dimensional surface model of the unit cell $p22_12$ symmetrized. The unit cell has been displaced by 49 Å (1/4 of the total length) in the direction of the longest crystallographic axis. The image shows two complete tetrameric structures. The asymmetrical unit cell has been marked with a white square. To show the relative orientations of the molecules, the lobes have been marked A, B, C. The protein placed at the upper side appears with its longest dimension lying down the crystal plane; the small lobe A is in front, and the lobes B and C are pointing downward. The molecule placed in the lower side has the longest dimension at an angle of ~60° with the crystal plane, showing the lobes A and B in the foreground and C downward. The scale bar represents 20 Å.

II molecules show a different ability to rearrange in SM or PC, lipids that differ only in their apolar region. A similar behavior has been reported for a number of negatively stained membrane proteins, where only those parts of the protein accessible to the aqueous solution were contrasted (Leonard et al., 1981, 1987; Ribi et al., 1988; Jap, 1989; Mitra et al., 1989). In some of these cases twofold screw axes are present in the crystal plane (Leonard et al., 1981, 1987). Furthermore, to verify this hypothesis, a 3D reconstruction was performed by application of the p2 symmetry. The structure obtained showed a unit cell composed of two "halves" of the tetramer (data not shown), which closely correlates with the upper half of the reconstruction in $p22_12$. Finally, the good agreement between the two protein views present in the asymmetric unit cell of the final 3D reconstruction confirms that the selection of the $p22_12$ two-sided plane group is correct.

3D model of sticholysin II and structural organization in tetrameric species

This work provides the first 3D image of a protein belonging to this family of cytolytic proteins. The results presented here are consistent with Stn II being a significantly asymmetrical molecule arranged in a three-lobe structure, with a maximum length of 51 Å and a width between the Y arms of 40 Å, this dimension being the same as the crystal thickness. It is also remarkable that Stn II, with 175 amino acids, is one of the smallest proteins reconstructed by this methodology.

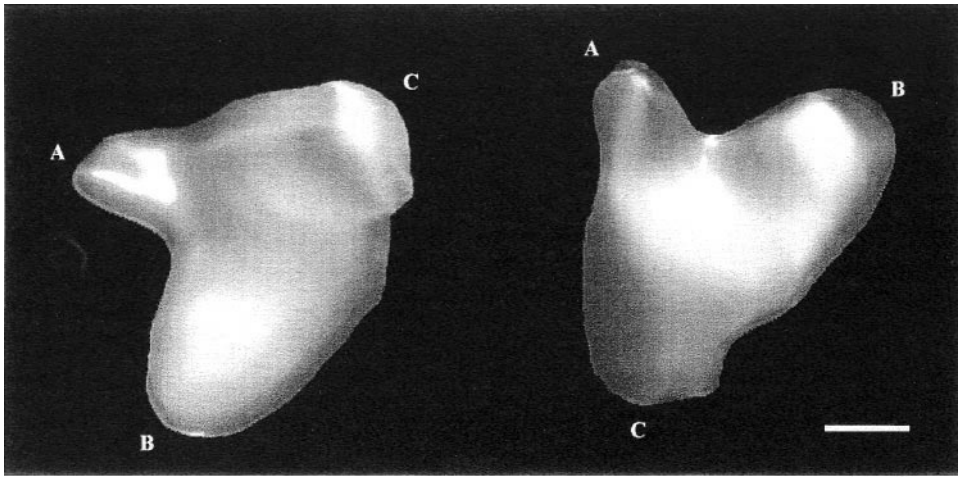

FIGURE 6 Two different views of the 3D surface model of Stn II, showing the concave and convex faces, respectively. The molecule appears to be Y-shaped, with a small curvature along its longest dimension. The lobes have been marked as in Fig. 5. The scale bar represents 12 Å

The structure formed by Stn II confirms the conclusions drawn from the projection maps, and it shows an arrangement that clearly resembles a tetrameric motif. In this regard, we have recently shown that Stn II behaves in solution like an associating monomer-tetramer system (de los Ríos et al., 1999), revealing the high tendency of the cytolysin to form discrete oligomers. However, the potential involvement of the tetrameric species present in solution in the mechanism of membrane interaction remains an open question at this moment. They may represent the precursor form of the competent pore that would result upon interaction with the membrane, as described for other toxins with a high β-structure content like that of Stn II (Thelestam et al., 1991; Walker et al., 1992; Vecsey-Semjen et al., 1996, 1997).

We are grateful to Dr. José L. Carrascosa and Dr. José M. Valpuesta for critical reading of the manuscript and valuable comments. We also thank Stavros Nicolopoulos for helpful discussions during the course of this work.

This work was partly supported by grants PB96-0602 and PB96-0601 from the Dirección General de Enseñanza Superior e Investigación Científica (Spain).

REFERENCES

Amos, L. A., R. Henderson, and P. N. T. Unwin. 1982. Three-dimensional structure determination by electron microscopy of two-dimensional crystals. *Prog. Biophys. Mol. Biol.* 39:183–231.

Baldwin, J. M., R. Henderson, E. Beckmann, and F. Zemlin. 202. 1988. Images of purple membrane at 2.8 Å resolution obtained by cryo-electron microscopy. *J. Mol. Biol.* 585–591.

Belmonte, G., G. Menestrina, C. Pederzolli, I. Krizaj, F. Gubensek, T. Turk, and P. Macek. 1994. Primary and secondary structure of a pore-forming toxin from the sea anemone *Actinia equina* L., and its association with lipid vesicles. *Biochim. Biophys. Acta.* 1192:197–204.

Belmonte, G., C. Pederzolli, P. Macek, and G. Menestrina. 1993. Pore formation by the sea anemone cytolysin equinatoxin II in red blood bells and model lipid membranes. *J. Membr. Biol.* 131:11–22.

Bernheimer, A. W. 1990. Cytolytic peptides of sea anemones. *In* Marine Toxins: Origin, Structure and Molecular Pharmacology. S. Hall and G. Strichartz, editors. American Chemical Society Symposium Series 418. Washington, DC. 304–311.

Bernheimer, A. W., and L. S. Avigad. 1976. Properties of a toxin from the sea anemone *Stoichactis helianthus*, including specific binding to sphingomyelin. *Proc. Natl. Acad. Sci. USA.* 73:467–471.

Blumenthal, K. M., and W. R. Kem. 1983. Primary structure of *Stoichactis helianthus* cytolysin III. *J. Biol. Chem.* 258:5574–5581.

Castañeda, O., V. Sotolongo, A. M. Amor, R. Stocklin, A. J. Anderson, A. L. Harvey, A. Engstrom, C. Wernstedt, and E. Karlsson. 1995. Characterization of a potassium channel toxin from the Caribbean Sea anemone *Stichodactyla helianthus. Toxicon.* 33:603–613.

Crowther, R. A., R. Henderson, and J. M. Smith. 1996. MRC image processing programs. *J. Struct. Biol.* 116:9–16.

de los Ríos, V., J. M. Mancheño, M. E. Lanio, M. Oñaderra, and J. G. Gavilanes. 1998. Mechanism of leakage induced on lipid model membranes by the hemolytic protein sticholysin II from the sea anemone *Stichodactyla helianthus. Eur. J. Biochem.* 252:284–289.

de los Ríos, V., J. M. Mancheño, A. Martínez del Pozo, C. Alfonso, G. Rivas, M. Oñaderra, and J. G. Gavilanes. 1999. Sticholysin II, a cytolysin from the sea anemone *Stichodactyla helianthus*, is a monomer-tetramer associating protein. *FEBS Lett.* 455:27–30.

Doyle, J. W., W. R. Kem, and F. A. Villalonga. 1989. Interfacial activity of an ion channel-generating protein from the sea anemone *Stichodactyla helianthus. Toxicon.* 27:465–471.

Fromherz, P. 1971. Electron microscopic studies from lipids films. *Nature.* 231:267–268.

Hardt, S., B. Wang, and M. F. Schmid. 1996. A brief description of I.C.E.: the integrated crystallographic environment. *J. Struct. Biol.* 116:68–70.

Harvey, H. L. 1990. Cytolytic toxins. *In* Handbook of Toxicology. W. T. Shier and D. Mebs, editors. Marcel Dekker, New York. 1–66.

Henderson, R., J. M. Baldwin, K. H. Downing, J. Lepault, and F. Zemlin. 1986. Structure of purple membrane from *Halobacterium halobium*: recording, measurement and evaluation of electron micrographs at 3.5 Å resolution. *Ultramicroscopy.* 19:147–178.

Hovmöller, S. 1992. CRISP: crystallographic image processing on a personal computer. *Ultramicroscopy.* 41:121–135.

Jap, B. K. 1989. Molecular design of PhoE porin and its functional consequences. *J. Mol. Biol.* 205:407–419.

Kem, W. R. 1988. Sea anemone toxins: structure and action. *In* The Biology of Nematocysts. D. A. Hessinger and H. F. Lenhoff, editors. Academic Press, New York. 375–405.

Kubalek, E. W., R. D. Kornberg, and S. A. Darst. 1991. Improved transfer of two-dimensional crystals from the air/water interface to specimen support grids for high-resolution analysis by electron microscopy. *Ultramicroscopy.* 35:295–304.

Leonard, K., H. Haiker, and H. Weiss. 1987. Three-dimensional structure of NADH: ubiquinone reductase (complex I) from *Neurospora* mitochondria determined by electron microscopy of membrane crystals. *J. Mol. Biol.* 194:277–286.

Leonard, K., P. Wingfield, T. Arad, and H. Weiss. 1981. Three-dimensional structure of ubiquinol:cytochrome *c* reductase from *Neurospora* mitochondria determined by electron microscopy of membrane crystals. *J. Mol. Biol.* 149:259–274.

Macek, P. 1992. Polypeptide cytolytic toxins from sea anemones (Actiniaria). *FEMS Microbiol. Immunol.* 105:121–129.

Macek, P., M. Zecchini, C. Pederzolli, M. Dalla Serra, and G. Menestrina. 1995. Intrinsic tryptophan fluorescence of equinatoxin II, a pore-forming polypeptide from the sea anemone *Actinia equina* L., monitors its interaction with lipid membranes. *Eur. J. Biochem.* 234:329–335.

Michaels, D. W. 1979. Membrane damage by a toxin from the sea anemone *Stoichactis helianthus.* I. Formation of transmembrane channels in lipid bilayers. *Biochim. Biophys. Acta.* 555:67–78.

Mitra, A. K., M. P. McCarthy, and R. M. Stroud. 1989. Three-dimensional structure of the nicotinic acetylcholine receptor and location of the major associated 43-kD cytoskeletal protein, determined at 22 Å by low dose electron microscopy and x-ray diffraction to 12.5 Å. *J. Cell. Biol.* 109:755–774.

Norton, R. S. 1991. Structure and structure-function relationships of sea anemone proteins that interact with the sodium channel. *Toxicon.* 29: 1051–1084.

Ribi, H. O., D. S. Ludwig, K. L. Mercer, G. K. Schoolnik, and R. D. Kornberg. 1988. Three-dimensional structure of cholera toxin penetrating a lipid membrane. *Science.* 239:1272–1276.

Shaw, P. J., and G. J. Hills. 1981. Tilt specimen in the electron microscope: a simple specimen holder and the calculation of tilt angles for crystalline specimens. *Micron.* 12:279–282.

Simpson, R. J., G. E. Reid, R. L. Moritz, C. Morton, and R. S. Norton. 1990. Complete amino acid sequence of Tenebrosin-C, a cardiac stimulatory and hemolytic protein from the sea anemone *Actinia tenebrosa. Eur. J. Biochem.* 190:319–328.

Taylor, K. A., and D. W. Taylor. 1993. Projection image of smooth muscle α-actinin from two-dimensional crystals formed on positively charged lipid layers. *J. Mol. Biol.* 230:196–205.

Tejuca. M., M. D. Serra, M. Ferreras, M. E. Lanio, and G. Menestrina. 1996. Mechanism of membrane permeabilization by sticholysin I, a cytolysin isolated from the venom of the sea anemone *Stichodactyla helianthus. Biochemistry.* 35:14947–14957.

Thelestam, M., A. Olofsson, L. Blomqvist, and H. Hebert. 1991. Oligomerisation of cell-bound staphylococcal alpha-toxin in relation to membrane permeabilisation. *Biochim. Biophys. Acta.* 1062:245–254.

Turk, T. 1991. Cytolytic toxins from sea anemones. *J. Toxicol. Toxin Rev.* 10:223–262.

Uzgiris, E. E., and R. D. Kornberg. 1983. Two-dimensional crystallization technique for imaging macromolecules, with application to antigen-antibody-complement complexes. *Nature.* 301:125–129.

Valpuesta, J. M., J. L. Carrascosa, and R. Henderson. 1994. Analysis of electron microscope images and electron diffraction patterns of thin crystals of ϕ29 connectors in ice. *J. Mol. Biol.* 240:281–287.

Varanda, W., and A. Finkelstein. 1980. Ion and non-electrolyte permeability properties of channels formed in planar lipid bilayer membranes by the cytolytic toxin from sea anemone *Stoichactis helianthus. J. Membr. Biol.* 55:205–211.

Vecsey-Semjen, B., S. Knapp, R. Mollby, and F. G. van der Goot. 1996. Partial C-terminal unfolding is required for channel formation by staphylococcal alpha-toxin. *J. Biol. Chem.* 271:8655–8660.

Vecsey-Semjen, B., C. Lesieur, R. Mollby, and F. G. van der Goot. 1997. Conformational changes due to membrane binding and channel formation by staphylococcal alpha-toxin. *J. Biol. Chem.* 272: 5709–5717.

Voges, D., R. Berendes, A. Burger, P. Demange, W. Baumeister, and R. Huber. 1994. Three-dimensional structure of membrane-bound annexin V. A correlative electron microscopy x-ray crystallography study. *J. Mol. Biol.* 238:199–213.

Walker, B., M. Krishnasastry, L. Zorn, and H. Bayley. 1992. Assembly of the oligomeric membrane pore formed by Staphylococcal alpha-hemolysin examined by truncation mutagenesis. *J. Biol. Chem.* 267: 21782–21786.

Zorec, R., M. Tester, P. Macek, and W. T. Mason. 1990. Cytotoxicity of equinatoxin II from the sea anemone *Actinia equina* involves ion channel formation and an increase in intracellular calcium activity. *J. Membr. Biol.* 118:243–249.